Journal of Low Temperature Physics, Vol. 95, Nos. 3/4, 1994

Formation of Layers and Gas and Liquid States of Helium in 8–13 Å Diameter Pores of Y Zeolites

Nobuo Wada

Institute of Physics, College of Arts and Sciences, University of Tokyo, Komaba, Tokyo 153, Japan

and

Hideyuki Kato* and Takashi Watanabe†

Department of Physics, Faculty of Science, Hokkaido University, Sapporo 060, Japan

(Received June 4, 1993; revised October 18, 1993)

Evolution of layers and their motional states for ^{3}He and ^{4}He adsorbed in Y zeolites have been studied by means of isosteric heat of sorption and heat capacity measurements. The two kinds of Y zeolites used in this study have pores interconnected in a ordered fashion, as well as the same diameter 8–13 Å. However, they are different potential profiles on the pore wall. The heat of sorption clearly shows localization potentials at Na^+ ion sites on the pore wall for Na–Y zeolites. In contrast, Silica–Y zeolite has few localization sites because it contains very few cations. We find that a solid layer forms on the pore wall at 38% of full pore adsorption amount for both Y zeolites. Upon increasing the amount adsorbed, the adatoms on the solid layer behave as a gas whose molar heat capacity is a half of the gas constant. From 50 to 65%, the second layer on the pore wall is in a semi-quantum liquid state since the heat capacity becomes proportional to temperature. Finally, the possibility of Fermi degeneracy of adsorbed ^{3}He in zeolitic micropores is discussed.

*Present address: National Research Laboratory of Metrology, Umezono 1-1-4, Tsukuba, Ibaraki 305, Japan.
†Present address: Kitanosawa 6-8-22, Minami-Ku, Sapporo 005, Japan.

0022-2291/94/0500-0507$07.00/0

1. INTRODUCTION

Helium adsorbed on solid surfaces[1,2] and into porous media[3-5] have generated much interest in recent years. This is due to the novel aspects of the adsorbed liquids and solids which are different from bulk ones. These properties are owing to not only the unique geometrical restriction but also adsorption potential of the substrates. Helium in porous media has been extensively studied using porous glasses whose pore diameter is larger than 50 Å for the superfluid transition of ^{4}He films.[4]

Zeolite provides much smaller pores which are typically less than 13 Å in diameter.[6] Unlike randomly connected porous glasses, the micropores of zeolites are orderly interconnected reflecting the crystal structure.

We have been studying ^{4}He and ^{3}He adatoms in micropores of zeolites and inspecting quantum properties of the adatoms.[7,8] In this paper, we present isosteric heat of sorption[9] and heat capacity of ^{3}He and ^{4}He adatoms in Silica–Y zeolite and Na–Y zeolite. These two types of zeolite have the same pore geometry. However, Na–Y zeolite contains Na^+ ion in its pore wall which alter the adsorption potential.

We find that the isosteric heat of sorption obtained from adsorption pressure and heat capacity measurements provides a clear picture of the adsorption potential in each zeolite. The dependence of isosteric heat of sorption on the amount of the adatoms gives the magnitude of the localization potential at Na^+ ion sites in Na–Y zeolite. The isosteric heat of sorption and low temperature heat capacity below about 4 K show formation of layers in the micropores. We discuss gas, liquid and solid states of the layers using the low temperature heat capacity. Also, possibilities of Fermi degeneracy of ^{3}He adatoms and Bose condensation of ^{4}He adatoms are examined by the heat capacity measurements down to 100 mK.

2. EXPERIMENTAL

2.1. Micropores of Y Zeolite

The Y zeolites used in this study are composed of aluminosilicate framework.[6] After a dehydration typically at 400°C in vacuum for 4–6 hours, the framework forms a three-dimensional (3D) network of cages connected through apertures making a diamond-like structure. Each cage is 13 Å in diameter. They are joined with four neighboring cages by apertures of 8 Å in diameter.

The chemical formula of Y zeolite is described as $M_x(AlO_2)_x(SiO_2)_y$ where M is a cation and $x + y = 192$. Zeolites with various $Al/Si = (x/y)$ ratios have been synthesized. Na–Y zeolite, Linde SK-40, that we used[8,10]

has the ratio Al/Si = 0.413. The Na^+ ions in the Na–Y zeolite cancel the negative charges of AlO_2^- which form electric dipoles with Na^+ ions. This ratio corresponds to seven electric dipoles per cage in the framework. The field gradients of the electric dipoles appearing on the pore wall are believed to act as a localization potential for the adatoms at the cation sites. Silica–Y zeolite, TSZ 380–HUA provided by Toso Co., Ltd.,[11] has a small ratio Al/Si = 0.014, which corresponds 0.33 $(AlO_2)^-$s per cage. Because of this small ratio, we expect little influence of the electric dipole fields on adsorption potential profiles of Silica–Y zeolite.

The amount of full adsorption n_{full} varies depending on manufacturers and cations existing in the pore. In order to determine n_{full}, we measured adsorption isotherms of ^{4}He at 4.2 K. As the adsorption amount n increases, the adsorption pressure p shows a sudden increase from near zero.[10] The amount n where the pressure starts increase gives n_{full}. The amount n_{full} for Na–Y zeolite was found to be 27.5 atoms/cage. The amount n_{full} for Silica–Y zeolite is 33 atoms/cage which is the largest among the Y zeolites we examined. The presence of few cations in Silica–Y zeolite appears to be contributing the large pore capacity.

In this paper, we use the percentage of full adsorption as an adsorption amount so as to compare the two Y zeolites.

2.2. Internal Energy of Adatoms

The internal energy U_s of adatoms in the micropores of zeolites has been obtained from results of adsorption pressure[9] and heat capacity measurements. When the helium gas in a sample cell and the helium adatoms into zeolitic pores are in equilibrium, the Clausius-Clapeyron equation for the adsorption pressure p is written as

$$\frac{dp}{dT} = \left(\frac{\partial S_g}{\partial n_g} - \frac{\partial S_s}{\partial n_s}\right) \Big/ \left(\frac{\partial V_g}{\partial n_g} - \frac{\partial V_s}{\partial n_s}\right) \tag{1}$$

where $\partial S/\partial n$ and $\partial V/\partial n$ are the differential molar entropy and volume, respectively.[9] The subscript g denotes gas phase in the sample cell while s is adatoms in the micropores. The isosteric heat q_{st} of sorption is defined as

$$\frac{q_{st}}{T} = \left(\frac{\partial S_g}{\partial n_g} - \frac{\partial S_s}{\partial n_s}\right) \tag{2}$$

Assuming the gas phase to be ideal at a low pressure, it satisfies the relation $\partial V_g/\partial n_g = RT/p$. Also assuming $\partial V_g/\partial n_g \gg \partial V_s/\partial n_s$, Eq. (1) becomes

$$q_{st} = -R \left.\frac{\partial \ln p}{\partial (1/T)}\right|_{n_s = \text{const}} \tag{3}$$

From the first law of thermodynamics and $dn = dn_s = -dn_g$, the change of the total energy $U_s + U_g$ due to adsorption dn is given by

$$\left(\frac{\partial U_s}{\partial n_s} - \frac{\partial U_g}{\partial n_g}\right) dn = -q_{st}\, dn - p\, dV_g \tag{4}$$

Since $\partial U_g/\partial n_g = (3/2)\, RT$ and $p\, dV_g = RT\, dn_g$, Eq. (4) gives

$$q_{st} = \frac{5}{2} RT - \frac{\partial U_s}{\partial n} \tag{5}$$

Hence, q_{st} gives the differential internal energy $\partial U_s/\partial n$ of the adatoms.

When the adsorption pressure in the sample cell becomes too small to be measured as the temperature decreases, we use heat capacity $C(n, T)$ to obtain temperature dependence of the internal energy U_s. U_s is described as

$$U_s(n, T) = U_s(n, T = 0\ \mathrm{K}) + \int_0^T C(n, T')\, dT' \tag{6}$$

From Eq. (6) and Eq. (5), q_{st} is written as

$$q_{st}(n, T) = \frac{5}{2} RT - \left.\frac{\partial U_s}{\partial n}\right|_{T=0\ \mathrm{K}} - \frac{\partial}{\partial n} \int_0^T C(n, T')\, dT' \tag{7}$$

Since the heat capacity data alone cannot determine the value of $\partial U_s/\partial n$ at $T = 0$ K, we obtained $\partial U_s/\partial n$ and q_{st} down to zero temperature by connecting the curve which is given by the heat capacity to the curve determined by the adsorption pressure measurement.

3. RESULTS AND DISCUSSIONS

3.1. Adsorption Potential on Pore Walls of Na–Y and Silica–Y Zeolites

Adsorption pressure p of ^{4}He in each Y zeolite has been measured down to 1 Pa at constant amounts n adsorbed. The results for Silica–Y zeolite are plotted as log p vs. $1/T$ in Fig. 1. Isosteric heat q_{st} of sorption, which is obtained from the derivative of the curve in Fig. 1 using Eq. (3), is shown with solid curves in Fig. 2. Below the temperature where p becomes too small to be measured, we have obtained q_{st} using the heat capacity results and Eq. (7), as shown with the dashed curves in Fig. 2. The n-dependence of $q_{st}(T = 0\ \mathrm{K})$ for ^{4}He in Silica–Y and that for Na–Y

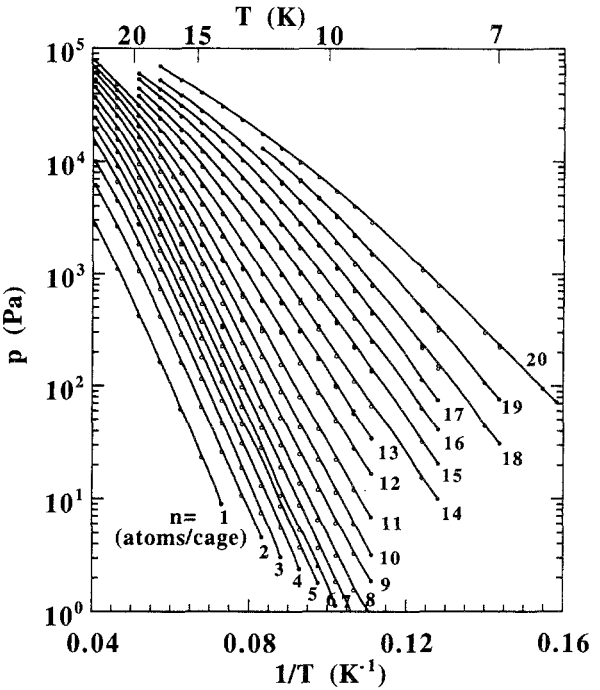

Fig. 1. Adsorption pressure p of ^{4}He against temperature T for Silica–Y zeolite as a function of adsorbed amount n.

zeolite[10] are shown together in Fig. 3, where n is normalized for the full pore amount n_{full}. Both curves show stepwise changes with increasing n; i.e., above $n = n_a$ and n_b marked with the arrows, $q_{st}(T = 0\ \text{K})$ becomes flat. The value of $q_{st}(T = 0\ \text{K})$ at n_a is 1.3 kJ/mol (156 K) for both Silica–Y and Na–Y zeolites. In the following, we consider $q_{st}(T = 0\ \text{K})$ at low n and stepwise change at n_a. The other stepwise change at $n = n_b$ is discussed in Sec. 3.4.

The state of adatoms for low n are mostly influenced by the potential from the framework. In the case of Na–Y zeolite with the ratio Al/Si = 0.413, the framework contains seven electric dipoles of Na^+ and $(AlO_2)^-$ per cage. The electric field gradient of the dipole appearing on the pore wall enhances the van der Waals potential. So there are localization sites at the cation whose adsorption potential is lower than that on the pore wall made of silicate (SiO_2). At zero temperature, the adatoms should localize at the cation sites. The potential energy at the cation site is estimated to be -1.6 kJ/mol using Eq. (5) and $q_{st}(T = 0\ \text{K}) = 1.6$ kJ/mol at the lowest n in Fig. 3. When the adatoms are adsorbed on all the localization sites, the excess adatoms will be on the silicate wall. The excess adatoms above n_a

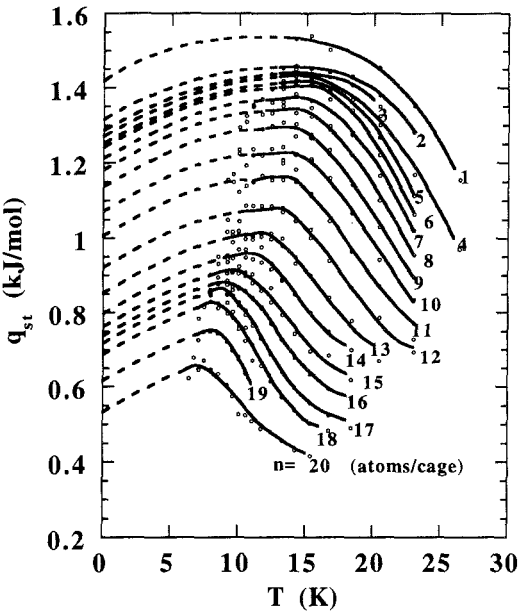

Fig. 2. Isosteric heat of sorption q_{st} at adsorbed amount n for Silica–Y zeolite. Open circles (solid curves) are obtained from the adsorption pressure measurement. Dashed curves are those obtained from the heat capacity data (see the text).

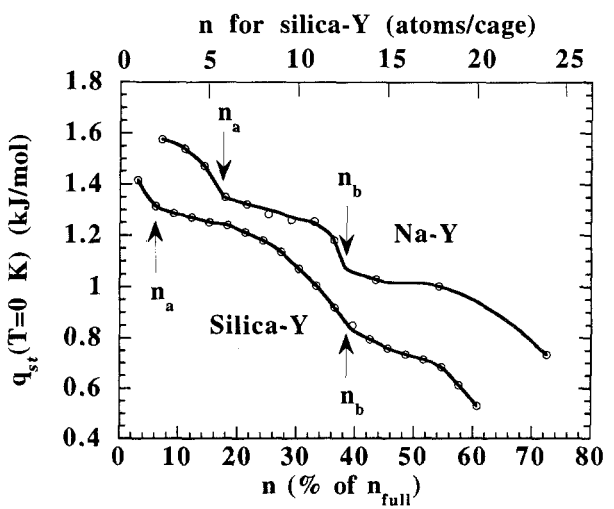

Fig. 3. Isosteric heat of sorption q_{st} at $T=0$ K of ^{4}He in Silica–Y and Na–Y zeolites. The amount n for Na–Y zeolite is normalized to the full pore amount n_{full} so as to compare with that of Silica–Y zeolite.

are likely to adsorb on the silicate wall. The potential at the silicate wall is estimated to be -1.3 kJ/mol, because the value of q_{st} at n_a is the same 1.3 kJ/mol for Na–Y zeolite as well as for Silica–Y zeolite whose pore wall is mostly composed of silicate. The depth of the localization potential for the Na^+ ion site is estimated to be 0.3 kJ/mol (35 K) which is the difference of $q_{st}(T=0\,\mathrm{K})$ between $n\sim 0$ and n_a for Na–Y zeolite. When Na^+ is exchanged by Ca^{2+} and H^+, $q_{st}(T=0\,\mathrm{K})$ at $n\sim 0$ depends on the kind of cation because of the different depth of localization potential.[12]

Existence of a similar n-dependence of q_{st} for Silica–Y zeolite below 1.5 atoms/cage (Fig. 3) indicates that there are some localization sites whose potential is lower than -1.3 kJ/mol of the average silicate wall.

3.2. Motional State of Helium Adatoms at High Temperatures

At high temperatures where adsorption pressure is observed as shown in Fig. 1, the helium adatoms are thermally excited from the lowest potential. The isosteric heat of sorption at high temperature, i.e., solid curves in Fig. 2, shows steep decrease with increasing temperature. The slope of the curve is $\sim 6R$ at 25 K for the smallest adsorbed amount $n=1$ atom/cage. This gives the differential internal energy of $\partial U_s/\partial n \sim 8.5RT + \text{constant}$ using Eq. (5).

Takaishi *et al.*[13] have studied Xe adsorbed in Ferrielite which has one-dimensional pores of 5 Å in diameter. Its isosteric heat of sorption at small amount adsorbed is constant to the temperature in the range 200–500 K, which gives $\partial U_s/\partial n = (5/2)\,RT + \text{constant}$. This internal energy is assigned to the 1D translation along the 1D pore and the classical 2D harmonic vibrations in the cross section whose thermal energies per mole are $\frac{1}{2}RT$ and $2RT$, respectively. The potential profile in Ferrielite can be described by a harmonic potential in the pore cross section whose minimum is at the center of the pore. The pore diameter of Ferrielite is 1.2 times larger than the Xe diameter of 4 Å. While, the cage diameter 13 Å of the Y zeolite is 5.2–4.3 times larger than the He adatom assuming 2.5–3 Å in diameter.

The potential in the void of zeolite can be calculated by summing interatom interactions between an adatom and all of the atoms composing the framework.[14] As a crude model we calculated the potential in the cross section of a cylindrical pore of 13 Å in diameter. We assumed the Lennard-Jones interaction taking the parameters of Silicate and helium atoms. The calculated potential in the cross section shows a deep minimum at about 1 Å from the pore wall, as in the case of the flat surface. The adsorption potential energy of -1.3 kJ/mol (-156 K) on the silicate wall for Y zeolite corresponds to the energy of the minimum value of the pore wall potential plus the zero point energy of ^{4}He adatom there. The zero point energy for

^{4}He is estimated to be 0.65 kJ/mol from the difference 0.1 kJ/mol of adsorption potential between ^{3}He and ^{4}He for Na–Y zeolite[10] and by assuming that the zero point energy is proportional to inverse square root of the mass. Then the depth of the minimum is roughly estimated to be -1.95 kJ/mol (-230 K). The potential at the center of the cross section is about 1/8 of the depth of minimum near the pore wall. This potential profile is quite different from the harmonic potential for Xe in Ferrielite, since Ferrielite has potential minimum at the center of the pore.

When we ignore interaction among adatoms at low n and use the classical distribution function, the molar internal energy is described by the sum of the kinetic energy of $(3/2)\,RT$ and the average potential energy $N\langle V\rangle$. The steep slope of q_{st} above 21 K at 1 atom/cage (Fig. 2) suggests $N\langle V\rangle \sim 7RT + \text{constant}$. This temperature dependence exceeds $1.5RT$ for a 3D harmonic potential. This excess dependence can be explained by thermal excitation of adatoms from the near-wall potential minimum to the center of the pores. This picture is consistent with the fact that the adsorption pressure starts increasing neat 15 K. The adatoms must be thermally distributed near the center of the pore before it comes out of zeolite, because the adsorption potential near the pore center is still lower than outside of zeolite. The low potential in the pore is also supported by the fact that the presser isotherm at 4.2 K cannot be observed up to the full adsorption.[10]

The thermal distribution in the pore and the gas-like properties suggests a large mobility of the He adatoms in the micropores. Its self diffusion coefficient has been measured using a pulsed NMR technique for the ^{3}He adatoms.[15] The coefficient in Na–Y zeolite has been found to be of the same order as that in the bulk liquid.

3.3. He Adatoms at Localization Sites

At zero temperature, the adatoms of the amount n_a are at the localization sites on the pore walls. Figure 3 gives n_a to be 1.5 atoms/cage and the depth of the localization potential about 0.12 kJ/mol (14 K) for Silica–Y zeolite. The temperature dependence of the heat capacity at 1 atom/cage, below n_a, is shown in Fig. 3. The whole dependence can be fitted by an Einstein model[16] as shown with the solid curve, which assumes the Einstein temperatures $\Theta_E^x = \Theta_E^y = 13$ K and $\Theta_E^z = 31$ K for the two directions along the wall and perpendicular to the wall, respectively.

An activation type dependence at the low temperatures is observed for Na–Y zeolite when the amount adsorbed is less than n_a. A typical activation energy is of the order of 5 K from the data below 2 K at $n = 7\%$ of

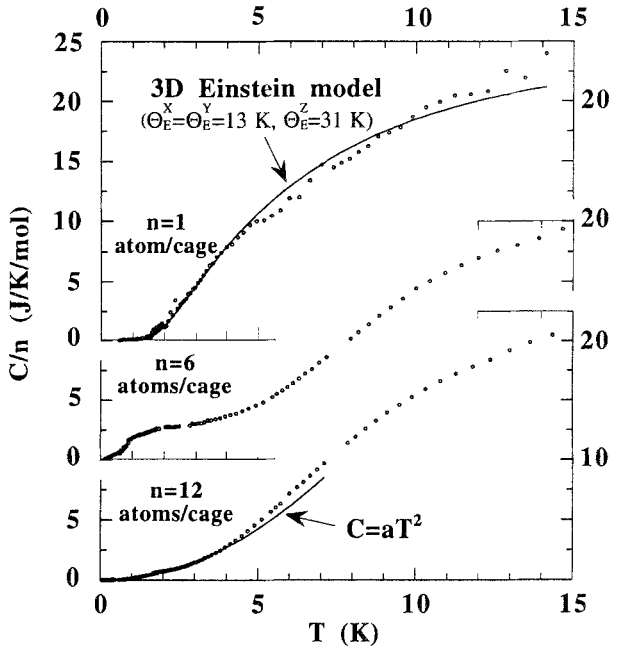

Fig. 4. Molar heat capacity C/n of ^{4}He in Silica–Y zeolite at $n \lesssim n_b$.

n_{full}. A larger activation energy is suggested from the heat capacity data for Ca–Y zeolite corresponding to the localization potential above 170 K[12] which is deeper than 35 K for Na–Y zeolite.

The temperature dependence above 2 K cannot be fitted by the Einstein model for the case of Na–Y zeolite, which is shown in Fig. 5(a) by plotting $C/n/T$ against T.[10] This shows an obvious cusp at $T_0 = 3.1$ K. T_0 varies from 3.6 to 1.9 K with increasing n, which appear to suggest a phase change. The number of localization sites is larger than that of Silica–Y zeolite. Direct transfer of adatoms among the sites is likely to play a role for the heat capacity anomaly at T_0 for Na–Y zeolite.

3.4. First Layer Completion at $n = n_b$

Figure 6 shows an isothermal heat capacity of ^{4}He adsorbed in Silica–Y zeolite where 1 atom/cage corresponds to 0.522 mmol of ^{4}He adsorbed in a sample cell. These finding has been shown in our preliminary report.[17] The dashed lines show $C = 3nR$ which assumes 3D classical thermal vibrations of the adatoms and $C = (5/2)\,nR$ of a classical 1D gas with

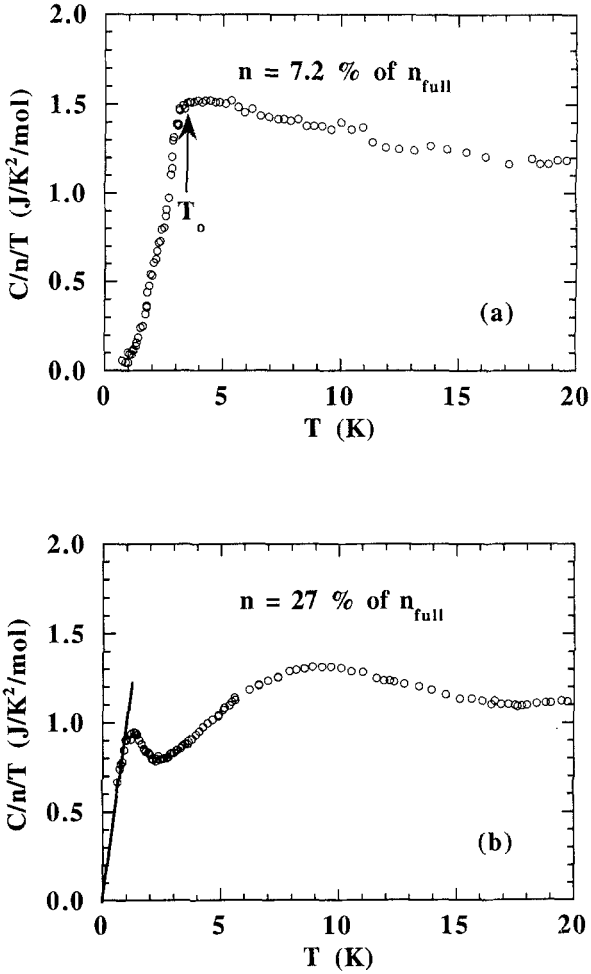

Fig. 5. $C/n/T$ vs. T of ^{4}He in Na–Y zeolite, (a): $n = 7.2\%$ of n_{full} as an example below n_a, and (b): $n = 27\%$ of n_{full} as an example between n_a and n_b.

2D classical harmonic vibrations. The dependence of $T = 15$ K is close to $C = 3nR$ below about n_a and approaches $C = (5/2)\,nR$ at larger amount of n. In contrast to the monotonic increase at $T = 15$ and 10 K, the isothermal curves at $T = 1$ and 2 K depends strongly on the amount adsorbed. The dependence shows minimum at the point n_b marked with the arrow. The minimum point is found to be 12.2 ± 0.2 atoms/cage which is 37% of n_{full}, from the isothermal $C - n$ curve below 1 K. A similar heat capacity minimum is observed when the first layer is completed on Graphite.[18]

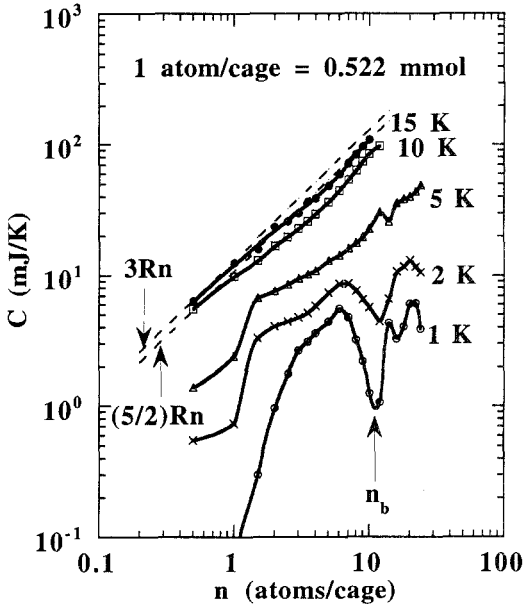

Fig. 6. Isothermal heat capacity C against n of ^{4}He adsorbed in Silica–Y zeolite. The adsorbed amount in the sample cell is 0.522 mmol for 1 atom/cage.

The minimum of the $C-n$ curve and the second stepwise change of $q_{st}(T=0\,\mathrm{K})$ (Fig. 3) occur at $n_b = 38\,\%$ of n_{full} for both Na–Y zeolite[10] and Silica–Y zeolite within experimental error. These results indicate that the first layer on the pore wall is completed at n_b. The value of $q_{st}(T=0\,\mathrm{K})$ at n_b is 0.85 kJ/mol (100 K) for Silica–Y zeolite and 1.05 kJ/mol (125 K) for Na–Y zeolite. The difference of q_{st} between n_a and n_b is 0.45 kJ/mol (54 K) and 0.25 kJ/mol (30 K) for Silica–Y and Na–Y zeolite, respectively. This suggests that the first layer formation is well defined at temperatures sufficiently below 54 or 30 K.

At the adsorbed amounts $n=n_b$ and just below n_b, the temperature dependencies of the heat capacity are proportional to T^2 for both Y zeolites. Figure 7(a) shows a heat capacity plotted against T^2 for Silica–Y zeolite at $n=12$ atoms/cage (12×0.522 mmol in the sample cell) which is just below n_b. This T^2-dependence and its small magnitude comparable to the heat capacity of the helium solid layer on graphite[18] suggests a 2D Debye solid state of the first layer at its completion.

The isothermal heat capacity curves at 1 and 2 K for Silica–Y zeolite (Fig. 6) have maximum between n_a and n_b. Also a similar maximum is observed for Na–Y zeolite.[10] At the adsorbed amount near the maximum,

the adatoms excess to n_a are positioned on the silicate wall, while the adatoms up to n_a are in the localization sites as discussed in Sec. 3.3. Corresponding heat capacity shows a hump around 2 K as shown in Fig. 4 for Silica–Y zeolite at $n = 6$ atoms/cage. The temperature dependencies no longer show the activation type dependence as seen at $n < n_a$. In case of Na–Y zeolite, between n_a and n_b, the heat capacity shows T^2-dependence at temperatures lower than 1 K.[8,10] The heat capacity at $n = 27\%$ of n_{full} is

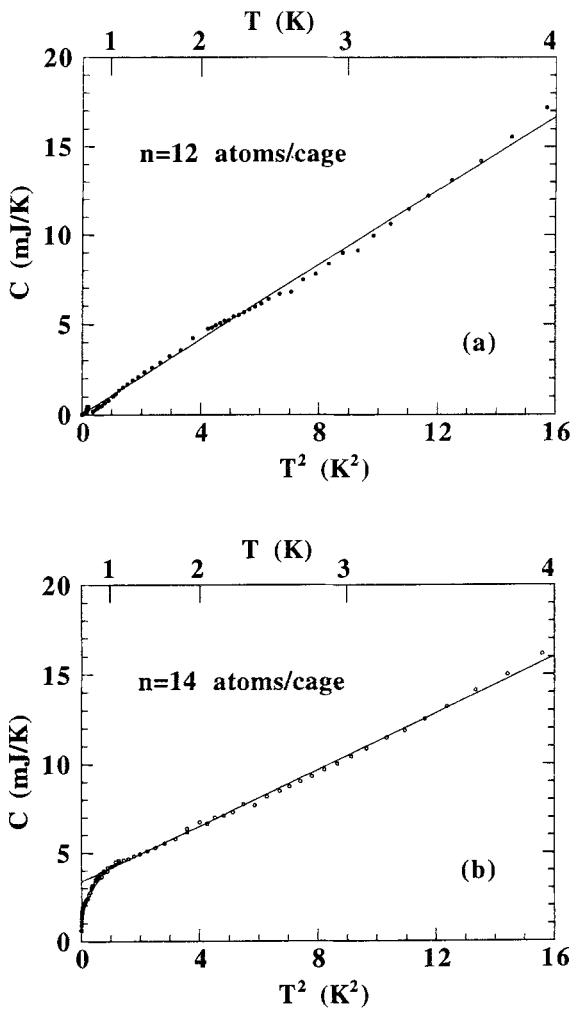

Fig. 7. C vs. T^2 of ^{4}He in Silica–Y zeolite, (a): $n = 12$ atoms/cage just below n_b, and (b): $n = 14$ atoms/cage above n_b, where 1 atom/cage = 0.522 mmol.

shown in Fig. 5(b) where the solid line describe the T^2-dependence. Its Debye temperature is obtained to be 14 and 10 K assuming two and one 2D phonon modes, respectively. The value 10 K is much smaller than the Debye temperature 20 K for the bulk liquid ^{4}He.

3.5. Gas and Liquid States of the Second Layer

The second stepwise change of $q_{st}(T=0\,\mathrm{K})$ occurs at $n_b = 38\%$ of n_{full} for both zeolites (Fig. 4). This suggests a small interaction among the adatoms of $n-n_b$ on the first solid layer of n_b. The temperature dependence of the heat capacity of ^{4}He adatoms in Silica–Y zeolite is shown in Fig. 7(b) for $n=14$ atoms/cage which corresponds $n-n_b = 1.8\pm0.2$ atoms/cage. The dependence can be described as $C=\beta+aT^2$ between 1 and 4 K. Since the T^2-dependence continues up to 4 K just below n_b (Fig. 7(a)), the T^2-term in Fig. 7(b) is of the first solid layer of the amount n_b. Applying the 2D Debye model with two phonon modes,[19] the value $a/n_b = 0.115\,\mathrm{J/K^3/mol}$ gives the Debye temperature to be $\Theta_D = 46$ K. The molar heat capacity of the second layer is estimated to be $\beta/(n-n_b) = 3.7\pm0.4\,\mathrm{J/K/mol}$. This magnitude is close to $R/2(=4.2\,\mathrm{J/K/mol})$ of a 1D classical gas where two motional freedoms per adatom are in a ground state and the other one freedom only contributes to the heat capacity. In the case of Na–Y zeolite, $\partial C/\partial n$ was observed to be $R/2$ in the same range $n_b < n \lesssim 45\%$ of n_{full} and at the same temperatures.[10] This He gas state in Y zeolites is unlike the 1D Xe gas in the 1D pores of Ferrielite[13] in the sense that the 2D classical vibration in the cross section gives the total energy per mole to be $(5/2)\,RT$, i.e., $\partial D/\partial n = (5/2)\,R$.

The interaction among the second layer adatoms becomes large at larger amount adsorbed. We consider the state of the second layer adatoms from the heat capacity by subtracting the first solid layer heat capacity C_1 from the data. For Silica–Y zeolite, we put $C_1 = aT^2$ where $a = 0.787\,\mathrm{mJ/K^3}$ from Fig. 7(b) and the amount of the first layer to be $n_b = 12.2$ atoms/cage. Then, the molar heat capacity C'/n' of the second layer adatoms is given by

$$C'/n' = (C-C_1)/(n-n_b) \tag{8}$$

The temperature dependence is shown in Fig. 8. This shows again the gas heat capacity of about $R/2$ at $n=14$ atoms/cage (42% of n_{full}). The dependencies at $n=18$ and 20 atoms/cage (54 and 60% of n_{full}) become almost proportional to temperature. The slopes of the solid lines are 1.3 and 1.1 $\mathrm{J/K^2/mol}$ for 18 and 20 atoms/cage, respectively.

Bulk ^{3}He and ^{4}He remain liquids at very low temperatures because of a large zero point motion. Andreev[20] has pointed out that these liquids

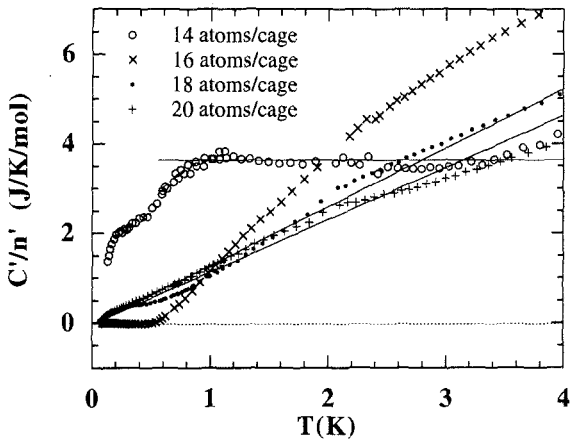

Fig. 8. C'/n' vs. T of ^{4}He in Silica–Y zeolite at $n > n_b$. C'/n' corresponds to the molar heat capacity of the second layer adatoms on the first solid layer (see the text).

behaves as a semi-quantum liquid which has the heat capacity proportional to temperature above quantum liquid region or solidification. The coefficient of bulk liquid ^{4}He is 2.3 J/K^2/mol at $2 \lesssim T \lesssim 9$ K and pressure 25 atm. The second layer adatoms with the T-linear heat capacity in Fig. 8 can be described by the semi-quantum liquid. Same T-linear dependence is observed for Na–Y zeolite between 50 and 65 % of n_{full}.[10] The coefficient of the T-linear heat capacity is a half of that of the bulk liquid ^{4}He.

The isothermal $C-n$ curve below few Kelvin becomes quite small near full adsorption.[10] Also, there is no clear indication of third layer formation in the heat capacity and q_{st} results. Considering the size of the cage and the hard core size of He adatom, there is little room left after first and second layer completion. The small molar heat capacity suggests a solid state of the adatoms.

3.6. Quantum Properties of ^{3}He and ^{4}He Adatoms

It still remains a question whether Fermi degeneracy of ^{3}He and superfluid of ^{4}He in the micropores can be observed. We have examined these possible quantum effects by heat capacity measurement below 1 K for ^{3}He and ^{4}He. The quantum effects can be expected to cause a qualitative difference of heat capacity between the Fermion and the Boson at sufficiently low temperature. Specifically, the Fermi degeneracy of ^{3}He adatoms should show a large heat capacity anomaly around the Fermi temperature.

In Y zeolites, the gas and liquid states of the second layer exist down to 1 K. Assuming the same first solid layer heat capacity as in Fig. 7(b), the molar heat capacity C'/n' defined by Eq. (8) of the second layer in Silica–Y zeolite are shown in Fig. 9 for ^{3}He and ^{4}He at $n = 15$ atoms/cage (45% of n_{full}). The heat capacity of ^{3}He clearly shows an anomaly below about 0.4 K. At $n = 15$ atoms/cage, there are average 2.8 atoms for the second layer per cage. The magnitude of the heat capacity anomaly of ^{3}He is $C'/n' = 2.4$ J/K/mol at $T \sim 0.2$ K. This is compared to submonolayer heat capacity of ^{3}He on Graphite[18] which shows Fermi degeneracy below 0.1 K. The ^{3}He submonolayer shows a hump of 1.5–2 J/K/mol in magnitude at $T \sim 0.1$ K. Similar heat capacity anomaly has been seen for ^{3}He in Na–Y zeolite as well at the adsorbed amounts 55–65% of n_{full}.[8]

In the measurement for ^{3}He in Silica–Y zeolite, thermal relaxation time of the sample cell becomes too long to measure by our apparatus at adsorbed amounts 45–60% of n_{full} and below 0.2–0.6 K which depends on n. So, data below 0.2 K could not be obtained at $n = 15$ atoms/cage (45%) in Fig. 9. The long relaxation time in the sample cell appears to be caused by large heat capacity of the ^{3}He adatoms.

The gas and liquid helium of the second layer exist in the micropores whose wall is covered with the first solid layer. The effective size of the cage for the second layer is 7 to 8 Å in diameter given the thickness of solid layer 2.5 to 3 Å. The aperture is as narrow as 2 to 3 Å in diameter. Fermi degeneracy in the micropores will show different features depending on how the transfer of second layer adatoms are influenced by the potential along the pore wall which is covered with the solid layer. The second layer

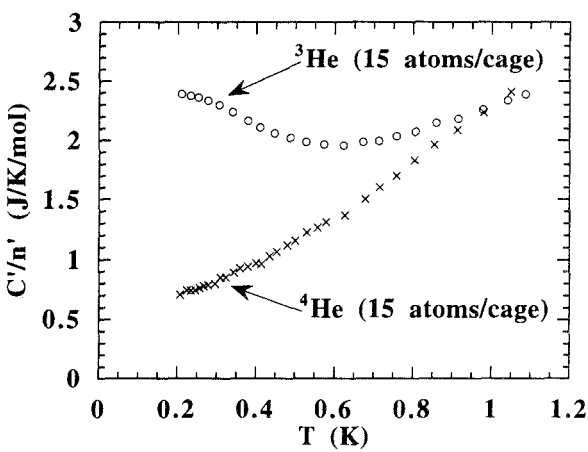

Fig. 9. C'/n' of ^{4}He and ^{3}He in Silica–Y zeolite at $n = 15$ atoms/cage (45% of n_{full}).

adatoms will show 3D Fermi degeneracy because of the 3D pore network, if there is no potential barrier. One of the possibilities is that there is a potential barrier at the aperture. Then, a few adatoms of the second layer are confined in each cage to make a quantum cluster at sufficiently low temperatures. Tasaki[21] has suggested that a theoretical calculation of a ^{3}He cluster consisted of three atoms yields a similar heat capacity anomaly as in Fig. 9. Further heat capacity and magnetic susceptibility studies are required to examine the possible quantum clusters.

At the same amount adsorbed and the temperatures as the ^{3}He Fermi degeneracy, it is expected superfluidity of the ^{4}He adatoms. However, in case of porous glasses,[22] the heat capacity anomaly associating the superfluid transition of ^{4}He films is too small to measure by the usual adiabatic heat pulse method.

4. CONCLUSIONS

In the 8–13 Å diameter pores of the Y zeolites, the adsorption potential for the helium adatoms and the evolution of layers are characterized by the isosteric heat of sorption and the heat capacity. The Na–Y zeolite has the localization site of about 35 K in depth which localize the adatoms of 15% of n_{full}. The Silica–Y zeolite localizes the adatoms of 4.5% of n_{full}. Despite the difference of potential profile, the first solid layer is completed at $n_b \sim 38\%$ of n_{full} for both Y zeolites. When ^{3}He or ^{4}He is adsorbed above n_b, the second layer is formed on the solid first layer. The second layer adatoms are in the gas state with the molar heat capacity $\partial C/\partial n \sim R/2$ down to $T \sim 1$ K at $38 < n \lesssim 45\%$ of n_{full}, and the liquid state with the T-linear heat capacity at $50 \lesssim n \lesssim 65\%$. The adatoms at the full pore have the small heat capacity compared with the gas and liquid states, which suggests a solid state of full adsorption.

Possibilities of the Fermi degeneracy of the ^{3}He and superfluidity of the ^{4}He gas/liquid-like adatoms are examined by measuring the heat capacity below 1 K. The qualitative difference of temperature dependence between ^{3}He and ^{4}He at $45 < n < 60\%$ of n_{full} suggests a Fermi degeneracy of the ^{3}He adatoms in the 3–8 Å diameter pores. It is possible that the quantum degeneracy shows three-dimensional or cluster characters reflecting topology and/or potential of the micropores.

ACKNOWLEDGMENT

We acknowledge S. Miyamoto for critical reading of the manuscript and stimulating discussions.

REFERENCES

1. R. E. Ecke, Q.-S. Shu, T. S. Sullivan, and O. E. Vilches, *Phys. Rev. B* **31**, 448 (1985); D. S. Greywall, *Phys. Rev. B* **41**, 1842 (1990).
2. D. J. Bishop and J. D. Reppy, *Phys. Rev. B* **22**, 5171 (1980).
3. M. Hiroi, T. Mizusaki, A. Hirai, T. Tunetoh, and K. Eguchi, *Jpn. J. Appl. Phys.* **26**, 289 (1987).
4. K. Shirahama, M. Kubota, S. Ogawa, N. Wada, and T. Watanabe, *Phys. Rev. Lett.* **64**, 447 (1990).
5. J. D. Reppy, *J. Low Temp. Phys.* **87**, 205 (1992).
6. D. W. Breck, *Zeolite Molecular Sieves* (Wiley, New York, 1974), Chap. 2.
7. H. Kato, K. Ishioh, N. Wada, T. Ito, and T. Watanabe, *J. Low Temp. Phys.* **68**, 321 (1987).
8. H. Kato, N. Wada, T. Ito, S. Takayanagi, and T. Watanabe, *J. Phys. Soc. Jpn.* **55**, 26 (1986).
9. D. M. Yang and A. D. Crowell, *Physical Adsorption of Gases* (Butterworths, London, 1962), Chap. 3.
10. N. Wada, K. Ishioh, and T. Watanabe, *J. Phys. Soc. Jpn.* **61**, 931 (1992).
11. Toso Co., Ltd., Akasaka 1-7-7, Minato-ku, Tokyo 107, Japan.
12. N. Wada, Yamamoto, T. Ito, and T. Watanabe, *New Developments in Zeolite Science and Technology*, Y. Murakami, A. Iijima, and J. W. Ward, eds. (Kodansha, Tokyo, 1986), p. 625.
13. T. Takaishi, K. Nonaka, and T. Okada, *J. Chem. Soc. Faraday Trans.* **83**, 3317 (1987).
14. D. H. Everett and J. C. Powl, *J. Chem. Soc. Faraday Trans. I* **72**, 619 (1976).
15. Kanada, N. Wada, T. Ito, K. Kumagai, and T. Watanabe, *Jpn. J. Appl. Phys.* **26**, 335 (1987).
16. C. Kittel and H. Kroemer, *Thermal Physics*, W. H. Freeman and Company, eds., 2nd ed., (1980), p. 83.
17. H. Kato, N. Wada, S. Miyamoto, T. Ito, and T. Watanabe, *Jpn. J. Appl. Phys.* **26**, 265 (1987).
18. M. Bretz, J. G. Dash, D. C. Hickernell, E. O. McLean, and O. E. Vilches, *Phys. Rev. A* **8**, 1589 (1973).
19. J. G. Dash, *Films on Solid Surfaces* (Academic Press, New York, 1975), p. 160.
20. A. F. Andreev, *Sov. Phys. JETP Lett.* **28**, 556 (1978).
21. S. Tasaki, to be submitted.
22. R. H. Tait and J. D. Reppy, *Phys. Rev. B* **20**, 997 (1979).